PAPER

Check for updates

Organic–inorganic interface engineering for integrated control of surface sites and hydrogen dynamics in chemoselective hydrogenation

Minji Yun,[b] Hyunjun Jeong,[a] Dongmin Lee[a] and Yongju Yun 🔵 *[ab]

Achieving high chemoselectivity in structure-sensitive heterogeneous hydrogenation reactions remains challenging, as conventional catalysts typically face a trade-off between selectivity and activity owing to competing adsorption and reaction pathways on metal surfaces. To address this, we report an interfacial organic grafting strategy that simultaneously regulates surface-site accessibility and hydrogen dynamics in Pt catalysts supported on non-reducible γ-Al$_2$O$_3$. Hexadecyltrimethoxysilane (HDTMS) is grafted onto the support surface prior to Pt deposition, generating Pt–HDTMS(x) catalysts with a low Pt loading of 0.5 wt%. Although HDTMS grafting significantly reduces the number of accessible Pt sites, the modified catalysts exhibit enhanced chemoselectivity and activity in acetophenone hydrogenation. Complete conversion with high chemoselectivity toward 1-phenylethanol is achieved under mild hydrogenation conditions, while undesired aromatic ring hydrogenation and overhydrogenation are effectively suppressed. Spectroscopic analyses reveal that HDTMS grafting selectively passivates well-coordinated Pt terrace sites while preserving under-coordinated sites that favor C=O hydrogenation. In parallel, hydrogen activation and spillover are promoted, leading to substantially increased turnover frequencies. The catalysts also show excellent stability under a wide range of hydrogen pressures and repeated cycling. These results demonstrate that organic–inorganic interface engineering provides an effective means to simultaneously enhance chemoselectivity and activity, enabling the rational design of efficient hydrogenation catalysts with low metal loadings.

Introduction

Chemoselective hydrogenation of multifunctional molecules represents a longstanding challenge in heterogeneous catalysis, because multiple reducible functional groups often compete for adsorption and activation on metal surfaces. Precise control over reaction pathways is critical in the synthesis of fine chemicals and pharmaceutical intermediates, where even minor side reactions can substantially reduce yield and process efficiency. Although heterogeneous catalysts demonstrate robustness, recyclability, and scalability, chemoselectivity is inherently difficult to achieve due to the strong dependence of adsorption modes and reaction pathways on the distribution of surface sites. Accordingly, catalyst design strategies that enable selective regulation of surface-site-dependent reactivity remain crucial in heterogeneous catalysis.

Hydrogenation reactions of multifunctional substrates containing carbonyl and olefinic or aromatic groups are widely used as structure-sensitive probe reactions, as their product distributions and reaction rates reflect the influence of surface geometry and hydrogen availability on catalytic behavior.[1–5] A prototypical example is acetophenone hydrogenation, in which selective carbonyl hydrogenation yields 1-phenylethanol, whereas hydrogenation of the aromatic ring leads to acetylcyclohexane and, upon further hydrogenation, 1-cyclohexylethanol. Owing to the strong surface-structure dependence of these competing pathways, acetophenone has been widely used as a benchmark substrate for probing chemoselectivity in heterogeneous hydrogenation catalysts.[6–9] Among various hydrogenation catalysts, Pt has been extensively studied for this reaction but typically exhibits limited selectivity toward carbonyl hydrogenation.[10–12] Attempts to increase the reaction rate, for example by increasing Pt loading or hydrogen pressure, often exacerbate this limitation by promoting aromatic-ring hydrogenation and overhydrogenation, thereby diminishing chemoselectivity.[13–16] More broadly, catalyst design strategies based on particle size control, alloying, and support modification have been actively explored, yet overcoming the chemoselectivity–activity trade-off remains challenging.[17–19]

At the molecular level, the chemoselectivity of acetophenone hydrogenation is governed by the geometric environments of metal active sites. Carbonyl groups preferentially adsorb on

[a]Department of Chemical Engineering, Pohang University of Science and Technology (POSTECH), Pohang, Gyeongbuk 37673, Republic of Korea. E-mail: yjyun@postech.ac.kr; Tel: +82-54-279-2398

[b]Division of Interdisciplinary Bioscience and Bioengineering, Pohang University of Science and Technology (POSTECH), Pohang, Gyeongbuk 37673, Republic of Korea

This journal is © The Royal Society of Chemistry 2026

J. Mater. Chem. A, 2026, **14**, 17445–17456 | 17445

under-coordinated (UC) sites such as edges and corners, whereas aromatic C=C bonds favor interaction with well-coordinated (WC) terrace sites.[20,21] Consequently, to selectively promote carbonyl hydrogenation while suppressing aromatic-ring saturation, catalysts must be designed to preserve access to UC sites while sterically blocking or deactivating WC sites. In other words, the relative population and accessibility of UC and WC sites considerably affect the reaction pathways and product distributions on Pt catalysts. Furthermore, the overall hydrogenation activity depends on the availability and transport of reactive hydrogen species on the catalyst surface.[22–25] These considerations highlight that both surface-site accessibility and hydrogen dynamics must be regulated to simultaneously achieve high chemoselectivity and activity.

Although organic surface modification and hydrogen spillover have each been explored as strategies to improve hydrogenation performance, their deliberate and concurrent regulation remains largely unexplored, particularly for catalysts supported on non-reducible oxides such as γ-Al$_2$O$_3$.[26–29] In many previous studies, organic modification has been implemented through ligand-modified metal surfaces, where organic molecules such as thiols or amines adsorb directly on metal nanoparticles to influence adsorption modes and catalytic selectivity.[30–33] In these systems, the organic species interact directly with metal active sites, and catalytic behavior is primarily regulated through ligand–metal interactions at the metal surface. Because the modifier is located directly on the metal, such approaches mainly alter the local adsorption environment of metal sites rather than intentionally controlling the architecture of the metal–support interface. Another widely explored strategy for modifying supported metal catalysts involves strong metal–support interaction, in which reducible oxide supports modify the structure and adsorption properties of metal nanoparticles through support reduction and partial encapsulation. Because this phenomenon relies on the reducibility of the oxide support, it is primarily observed for catalysts supported on reducible oxides such as TiO$_2$.[11,34,35]

In contrast to these approaches, the present work adopts a strategy in which organic species are grafted onto the oxide support prior to metal deposition. Specifically, hexadecyltrimethoxysilane (HDTMS) is introduced onto γ-Al$_2$O$_3$ before Pt deposition to construct a metal–organic–support interfacial architecture. This design is intended to selectively passivate WC Pt sites while preserving UC Pt sites and to influence hydrogen activation and migration at the catalyst surface. Here, we examine whether introducing grafted organic species at the metal–support interface can simultaneously control Pt surface-site accessibility and hydrogen dynamics during catalytic hydrogenation. To this end, systematic catalytic evaluation combined with spectroscopic analyses is employed to probe how interfacial organic modification influences hydrogen-mediated reaction pathways, with particular attention to promoting selective carbonyl hydrogenation while suppressing undesired aromatic ring hydrogenation and over-hydrogenation under conditions that typically favor these pathways in conventional Pt catalysts. Through this approach, we aim to establish organic–inorganic interface engineering as

a catalyst design strategy for jointly tuning surface-site accessibility and hydrogen dynamics to address the selectivity–activity trade-off in structure-sensitive hydrogenation catalysis.

Experimental

Chemicals and materials

The following reagents were used for preparing the HDTMS-grafted Pt catalysts: γ-Al$_2$O$_3$ (Puralox SCCa 5-150, Sasol) served as the support, and platinum(II) acetylacetonate (Pt(acac)$_2$, 98%, Acros) was used as the metal precursor. HDTMS (Sigma-Aldrich) and toluene (99.5%, Samchun Pure Chemical) were used for the grafting treatment. Acetophenone (99%, Alfa Aesar) and ethanol (99.9%, Samchun Pure Chemical) were used as the reactant and solvent, respectively, for the chemoselective hydrogenation tests.

Catalyst preparation

The HDTMS-grafted γ-Al$_2$O$_3$ supports were synthesized as follows: γ-Al$_2$O$_3$ (1 g) was dispersed in anhydrous toluene (70 mL) containing 0.3, 3, or 30 μmol of HDTMS and refluxed at 403 K for 12 h under an Ar atmosphere. The solid products were collected by filtration, washed with ethanol, and dried at 353 K. For Pt deposition, the HDTMS-grafted supports were suspended in an acetone solution of Pt(acac)$_2$, and the solvent was removed by evaporation at 313 K under stirring at 200 rpm, yielding a nominal Pt loading of 0.5 wt%. The resulting powders were dried at 353 K for 12 h and subsequently heat-treated under an Ar environment at 523 K for 3 h. The catalysts prepared in this manner were denoted as Pt–HDTMS(x), where x represents the amount of HDTMS used for grafting. A reference catalyst, Pt–HDTMS(0), was prepared using pristine γ-Al$_2$O$_3$ without HDTMS treatment, following the same impregnation and heat-treatment procedures to achieve a Pt loading of 0.5 wt%. In addition, a series of yPt–HDTMS(0) catalysts with various Pt loadings (y = 1, 3, 5, and 10 wt%) were synthesized using the same method with ungrafted γ-Al$_2$O$_3$.

Characterization

The textural properties of the catalysts were examined by N$_2$ physisorption at 77 K using a Micromeritics ASAP 2010 instrument after degassing the samples under vacuum at 473 K for 12 h. The Pt loadings of the Pt–HDTMS(x) catalysts were determined by inductively coupled plasma-optical emission spectroscopy (ICP-OES) using a SPECTRO ARCOS FHM22 analyzer. CO chemisorption measurements were conducted at 323 K on a MicrotracBEL BELCAT-II system equipped with a thermal conductivity detector. Prior to analysis, the samples were reduced in flowing H$_2$ at 473 K for 2 h. The Pt particle size (d_{CO}) was calculated assuming a CO/Pt adsorption stoichiometry of 1. The fraction of surface-accessible Pt sites (Pt_{avail}) was determined from the ratio of chemisorbed CO to the total Pt content. Scanning transmission electron microscopy (STEM) and energy-dispersive X-ray spectroscopy (EDS) mapping were performed using a JEOL JEM-2100F microscope. X-ray diffraction (XRD) patterns were collected on a Rigaku Ultima IV

17446 | J. Mater. Chem. A, 2026, **14**, 17445–17456

This journal is © The Royal Society of Chemistry 2026

diffractometer with Cu Kα radiation, operated at 40 kV and 20 mA over a 2θ range of 10–90°. The carbon content in the Pt–HDTMS(x) samples was quantified by elemental analysis using a vario MICRO cube instrument. Fourier transform infrared (FTIR) spectra were obtained using a Thermo Fisher Nicolet iS50 spectrometer with KBr-pelletized samples. Transmittance spectra were recorded in the range of 500–4000 cm^{-1} at a resolution of 4 cm^{-1} with 128 scans. Diffuse reflectance infrared Fourier transform (DRIFT) spectra were also collected on the same instrument. For CO-adsorbed DRIFT measurements, the catalysts were pre-reduced at 473 K under 5% H$_2$/Ar for 2 h, cooled to 323 K, and subsequently exposed to CO. H$_2$ temperature-programmed desorption (H$_2$-TPD) experiments were performed on a MicrotracBEL BELCAT-II analyzer equipped with a thermal conductivity detector. A 50 mg sample was reduced at 473 K for 2 h in flowing H$_2$, cooled to 323 K, and purged with Ar for 30 min prior to heating from 323 K to 1073 K at 10 K min^{-1} under Ar flow. To evaluate hydrogen activation, Pt–HDTMS(x) catalysts were mixed with WO$_3$ and treated at 473 K for 2 h in 5 vol% H$_2$/Ar. Using monochromatic Al Kα radiation (1486.6 eV), X-ray photoelectron spectroscopy (XPS) was performed at the Korea Basic Science Institute (KBSI) in Busan. All spectra were calibrated to the C 1s peak at 284.6 eV.

Catalytic performance tests

Prior to the hydrogenation reaction, the catalysts were pre-reduced under 5 vol% H$_2$/Ar at 473 K for 2 h. Catalytic tests at ambient hydrogen pressure were performed in a 100 mL three-neck round-bottom flask at 298 K under 0.1 MPa of H$_2$. High-pressure evaluations were performed in a stainless-steel reactor equipped with a 100 mL glass liner at 298 K under H$_2$ pressures of 0.5–5.0 MPa. In a typical run, 30 mg of the Pt catalyst was dispersed in 8 mL of ethanol, and the reactor was purged with H$_2$ for 10 min under stirring. The reaction was initiated by adding 2 mL of an ethanol solution containing 0.17 mmol of acetophenone. After the reaction, the catalyst was removed using a syringe filter, and the liquid products were analyzed using a Younglin YL6500 gas chromatograph equipped with a flame-ionization detector and a chiral capillary column (Chirasil-Dex CB, CP7502, Agilent). The turnover frequency (TOF) was calculated using eqn (1), considering initial conversions below 12%.

$$\text{TOF } (\text{h}^{-1}) = \frac{X_{\text{substrate}} \times n_{\text{substrate}} \times V}{\text{CO}_{\text{ads}} \times s \times m \times t} \qquad (1)$$

where $X_{\text{substrate}}$ denotes the conversion, $n_{\text{substrate}}$ is the number of moles of substrate, V is the molar gas volume under standard conditions (22 414 cm^3 mol^{-1}), CO$_{\text{ads}}$ is the amount of chemisorbed CO, s is the CO/Pt adsorption stoichiometry, m is the catalyst mass, and t is the reaction time.

Chemoselectivity was determined using eqn (2):

$$\text{Chemoselectivity } (\%) = \frac{n_i}{\sum\limits_{\text{product}} n_i} \times 100\% \qquad (2)$$

where n_i represents the number of moles of product i. All catalytic experiments were performed three times to ensure reproducibility. The standard deviations were within 0.7% for conversion and 0.6% for chemoselectivity.

Results and discussion

Structural and surface characterization of Pt–HDTMS(x) catalysts

HDTMS grafting onto γ-Al$_2$O$_3$ proceeded through condensation reactions between the silane groups and surface hydroxyls. The grafted supports were subsequently impregnated with a Pt precursor to obtain Pt–HDTMS(x) catalysts with a nominal Pt loading of 0.5 wt%, where x (0–30 μmol) represents the amount of HDTMS used for grafting. This HDTMS loading range was selected to systematically investigate how surface coverage influences Pt surface accessibility and hydrogen-related interfacial effects. Excessive grafting amounts, such as 50 μmol, hindered Pt deposition and resulted in negligible hydrogenation activity. Therefore, HDTMS loadings above 30 μmol were excluded from further investigation.

The textural properties of the catalysts were examined by N$_2$ physisorption. All samples exhibited type IV adsorption–desorption isotherms with H1 hysteresis loops, characteristic of mesoporous γ-Al$_2$O$_3$ (Fig. S1). The Brunauer–Emmett–Teller (BET) surface area of the ungrafted Pt–HDTMS(0) catalyst was 153 m^2 g^{-1}, whereas the HDTMS-treated samples displayed lower surface areas, consistent with partial occupation of surface sites by the grafted silane species (Table 1). As the HDTMS loading increased from 0.3 to 30 μmol, the BET surface area decreased from 129 to 108 m^2 g^{-1}, indicating progressively greater coverage of the Al$_2$O$_3$ surface by the grafted silane groups.

The measured Pt loadings of the Pt–HDTMS(x) catalysts were consistent with the intended nominal values (Table 1). The slightly lower loadings observed for Pt–HDTMS(3) and Pt–HDTMS(30) may be ascribed to partial blockage of γ-Al$_2$O$_3$ surface anchoring sites by the grafted HDTMS species. STEM analysis showed that Pt nanoparticles (NPs) were uniformly dispersed across all samples, with an average particle size of approximately 1.3 nm (Fig. 1). Consistent with these observations, the XRD patterns did not show any diffraction peaks attributable to metallic Pt, indicating that the size of Pt crystallites remained below the XRD detection limit and that they were well dispersed on the HDTMS-modified γ-Al$_2$O$_3$ supports (Fig. S2). Elemental mapping of Pt–HDTMS(30) revealed homogeneous distributions of Pt and carbon species, with the latter originating from the grafted HDTMS. This result confirmed the uniform distribution of the grafted silane moieties across the catalyst surface (Fig. S3).

The amount of grafted HDTMS was quantified from the carbon content originating from the silane species, as determined by elemental analysis (Table 2). Unlike the ungrafted Pt–HDTMS(0) sample, which displayed a negligible carbon content, the HDTMS-grafted catalysts showed carbon contents increasing from 3.8 to 8.5 wt% as the HDTMS loading increased from 0.3 to 30 μmol. This moderate increase reflects the saturation behavior characteristic of silane grafting on supports with a limited number of surface hydroxyl sites. Only the

This journal is © The Royal Society of Chemistry 2026

J. Mater. Chem. A, 2026, **14**, 17445–17456 | **17447**

Table 1 BET surface areas, Pt loadings, and physicochemical properties of Pt−HDTMS(x) catalysts

Sample	Surface area^a (m^2 g^{-1})	Pt^b (wt%)	d_{STEM}^{c} (nm)	Pt_{avail}^{d}	d_{CO}^{d} (nm)
Pt−HDTMS(0)	153	0.4	1.3	0.53	2.2
Pt−HDTMS(0.3)	129	0.4	1.3	0.12	7.0
Pt−HDTMS(3)	111	0.3	1.3	0.04	23.6
Pt−HDTMS(30)	108	0.3	1.3	0.03	34.4

^{a} BET surface areas obtained from N$_2$ physisorption. ^{b} Pt loadings measured using ICP-OES. ^{c} Pt particle sizes determined by STEM. ^{d} Pt_{avail} and d_{CO} obtained from CO chemisorption measurements.
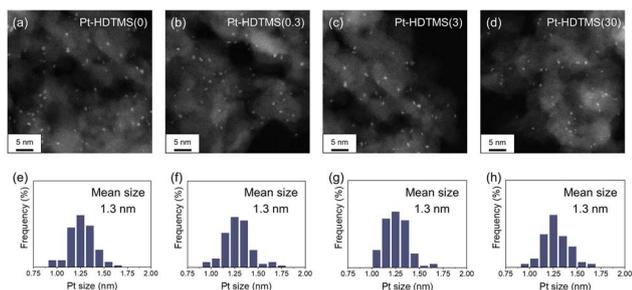

Fig. 1 STEM images (a–d) and corresponding size distributions (e–h) of Pt NPs on Pt−HDTMS(x) catalysts: (a) and (e) Pt−HDTMS(0); (b) and (f) Pt−HDTMS(0.3); (c) and (g) Pt−HDTMS(3); and (d) and (h) Pt−HDTMS(30).

Table 2 Carbon contents of Pt−HDTMS(x) catalysts

Sample	C^a (wt%)
Pt−HDTMS(0)	—
Pt−HDTMS(0.3)	3.8
Pt−HDTMS(3)	6.3
Pt−HDTMS(30)	8.5

^{a} Carbon content determined by elemental analysis.

fraction of HDTMS that can react with surface hydroxyl groups becomes covalently grafted, while the excess remains unreacted or is removed during washing. To identify the organic moieties introduced by HDTMS, FTIR transmittance spectra were collected for the Pt−HDTMS(x) catalysts (Fig. 2). All samples exhibited bands at 3450 and 1633 cm^{-1}, assigned to the bending modes of surface hydroxyl groups on Al$_2$O$_3$. The intensity of these vibrations gradually decreased with increasing HDTMS amount, indicating the progressive
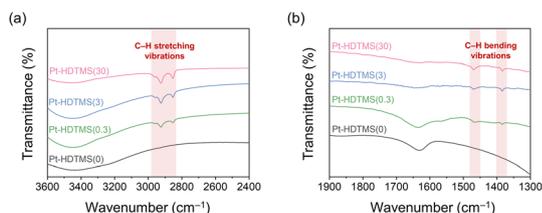

Fig. 2 FTIR transmittance spectra of Pt−HDTMS(x) catalysts over the ranges of (a) 3600–2400 cm^{-1} and (b) 1900–1300 cm^{-1}.

consumption of surface hydroxyls during silylation.[36–38] In addition, the HDTMS-grafted catalysts exhibited new absorption features at 2956, 2923, 2851, 1463, and 1385 cm^{-1}, corresponding to C–H stretching and bending vibrations. These bands were also observed in the spectrum of pure HDTMS (Fig. S4), verifying that the characteristic alkyl groups of HDTMS were incorporated onto the Al$_2$O$_3$ surface. The corresponding peak intensities increased with HDTMS loading, demonstrating that larger amounts of alkyl-containing HDTMS species were anchored to the support. These results confirm that HDTMS was successfully grafted onto the Al$_2$O$_3$ surface in the form of alkyl-functional silane species.

The grafted HDTMS species were expected to partially passivate the surface of the impregnated Pt NPs, thereby impeding reactant adsorption. The influence of HDTMS grafting on the accessibility of catalytically active Pt sites was examined by CO chemisorption using the Pt−HDTMS(x) samples (Table 1). Specifically, Pt_{avail} was determined from the amount of chemisorbed CO, assuming a 1 : 1 CO/Pt adsorption stoichiometry. Pt_{avail} was calculated as the ratio of CO-accessible Pt atoms to the total Pt amount measured by ICP-OES, representing the fraction of surface Pt not blocked by the grafted HDTMS species. The ungrafted Pt−HDTMS(0) catalyst exhibited a Pt_{avail} of 0.53 with d_{CO} = 2.2 nm, where d_{CO} denotes the Pt NP size determined by CO chemisorption. In contrast, Pt_{avail} decreased sharply to 0.12–0.03 with increasing HDTMS loading, indicating that the grafted HDTMS species substantially restricted access of CO to Pt surface sites. Because fewer CO probe molecules could adsorb onto the Pt surface, the calculated d_{CO} values increased markedly to 7.0–34.4 nm, despite the actual NP size being 1.3 nm, as measured by STEM (d_{STEM}). This mismatch between d_{CO} and d_{STEM} indicates that HDTMS introduces surface-bound organic species that increasingly cover the Al$_2$O$_3$ surface at higher grafting amounts, consistent with the elemental analysis and FTIR results.

Performance of Pt–HDTMS(x) catalysts in acetophenone hydrogenation

Acetophenone hydrogenation was selected as a probe reaction to assess the catalytic performance of the Pt−HDTMS(x) catalysts. Acetophenone contains both C=O and C=C functionalities, and its hydrogenation over Pt can proceed through multiple pathways, yielding 1-phenylethanol via C=O hydrogenation, acetylcyclohexane from aromatic ring hydrogenation, and 1-cyclohexylethanol through either C=O hydrogenation
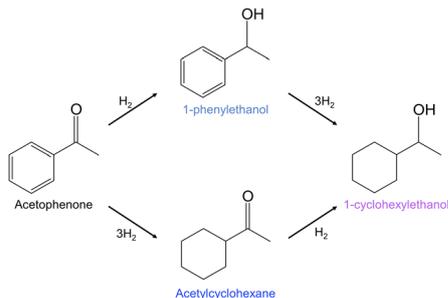
Scheme 1 Reaction pathways of acetophenone hydrogenation over Pt catalysts.

followed by ring hydrogenation or the reverse sequence (Scheme 1). Because the product distribution is sensitive to the surface environment of Pt catalysts, acetophenone hydrogenation provides a suitable platform for examining the effect of HDTMS-based surface modification on catalytic behavior. In this study, the reaction was directed toward selective C=O hydrogenation to produce 1-phenylethanol as the primary product, a high-value compound that serves as an important intermediate for downstream transformations.

To evaluate the performance of Pt–HDTMS(x) catalysts, the conversion of acetophenone and chemoselectivity toward 1-phenylethanol were measured as functions of reaction time (Fig. 3). For all samples, the conversion increased nearly linearly with reaction time over the initial reaction period. After 3 h, the ungrafted Pt–HDTMS(0) catalyst exhibited a conversion of only 34.7%, whereas the HDTMS-grafted catalysts showed substantially higher conversions, ranging from 65.6% to 100% depending on the HDTMS loading. Notably, the conversion increased progressively as the grafted HDTMS amount increased from 0.3 to 30 μmol. After 24 h, the ungrafted Pt–HDTMS(0) sample achieved only 63.7% conversion, while all HDTMS-grafted catalysts achieved complete conversion (100%). These results demonstrate that HDTMS grafting effectively

promotes catalytic activity under the present reaction conditions, despite the marked decrease in Pt_{avail}, as evidenced by CO chemisorption.

For the Pt–HDTMS(x) catalysts, the chemoselectivity toward 1-phenylethanol remained constant throughout the reaction and even after full conversion, indicating that overhydrogenation was suppressed. Compared with the ungrafted Pt–HDTMS(0) catalyst, which exhibited a chemoselectivity of only 46.3%, the HDTMS-grafted catalysts displayed substantially higher values that increased steadily with HDTMS loading. In particular, Pt–HDTMS(30) achieved the highest chemoselectivity of 88.5%. Product analysis revealed that the ungrafted Pt–HDTMS(0) catalyst produced 1-phenylethanol and acetylcyclohexane in a largely unselective manner (Fig. S5). In contrast, HDTMS grafting redirected the reaction toward selective C=O hydrogenation rather than aromatic ring hydrogenation, resulting in predominant formation of 1-phenylethanol and suppressed production of acetylcyclohexane. These results demonstrate that HDTMS grafting enhances both catalytic activity and chemoselectivity, thereby directing the reaction toward the desired pathway.

To benchmark the effect of HDTMS grafting against the conventional strategy of increasing Pt loading to achieve high conversion, the catalytic performance of ungrafted Pt–HDTMS(0) catalysts containing 1–5 wt% Pt was evaluated under identical reaction conditions and compared with the Pt–HDTMS(x) catalysts with the nominal 0.5 wt% Pt loading (Fig. 4). As expected, the yPt–HDTMS(0) catalysts (y = Pt loading in wt%) exhibited progressively higher conversion with increasing Pt loading owing to the greater number of active sites, ultimately reaching 100% conversion within 3 h for 5Pt–HDTMS(0). Notably, however, the catalytic activity of Pt–HDTMS(30), containing only 0.5 wt% Pt, was comparable to that of 3Pt–HDTMS(0), which contains six times more Pt. These results highlight that HDTMS grafting enables a substantial enhancement in intrinsic catalytic performance.
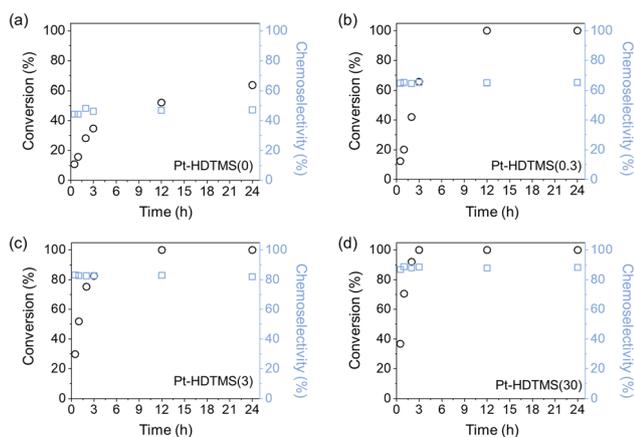

Fig. 3 Conversion and chemoselectivity as function of reaction time during acetophenone hydrogenation over Pt–HDTMS(x) catalysts: (a) Pt–HDTMS(0), (b) Pt–HDTMS(0.3), (c) Pt–HDTMS(3), and (d) Pt–HDTMS(30).
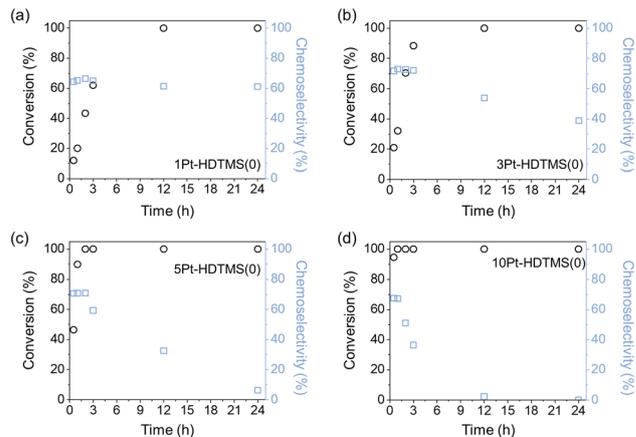

Fig. 4 Conversion and chemoselectivity as functions of reaction time during acetophenone hydrogenation over yPt–HDTMS(0) catalysts: (a) 1Pt–HDTMS(0), (b) 3Pt–HDTMS(0), (c) 5Pt–HDTMS(0), and (d) 10Pt–HDTMS(0).

This journal is © The Royal Society of Chemistry 2026

J. Mater. Chem. A, 2026, **14**, 17445–17456 | **17449**

Despite their high activity, all yPt–HDTMS(0) catalysts exhibited lower maximum chemoselectivity (≤73.2%) compared with Pt–HDTMS(30), which displayed a value of 88.5%. Moreover, the yPt–HDTMS(0) samples showed their highest chemoselectivity only at early reaction stages, followed by a sharp decline when approaching full conversion, with the loss of selectivity becoming more pronounced at higher Pt loadings. This loss of selectivity is attributable to overhydrogenation in the absence of surface modification, which leads to the formation of 1-cyclohexylethanol as the dominant product. In contrast, the Pt–HDTMS(x) catalysts maintained high chemoselectivity throughout the reaction, even after complete conversion. These results demonstrate that HDTMS grafting not only enhances catalytic activity at low Pt loadings but also suppresses C═C ring hydrogenation, enabling concurrent improvements in activity and chemoselectivity toward C═O hydrogenation to form 1-phenylethanol. These simultaneous gains cannot be achieved simply by increasing the Pt loading.

To further clarify the benefits of HDTMS grafting, the influence of hydrogen pressure on catalytic activity and chemoselectivity was evaluated using Pt–HDTMS(0) and Pt–HDTMS(30) as representative catalysts (Fig. 5). Increasing hydrogen pressure is a commonly used strategy to improve conversion by elevating the surface concentration of activated hydrogen species, a parameter that can also influence hydrogen transfer on the catalyst surface. The ungrafted Pt–HDTMS(0) catalyst exhibited a pressure-dependent increase in conversion, reaching 100% conversion at 3.0 MPa within 3 h. However, this enhancement in activity did not lead to any improvement in chemoselectivity. The chemoselectivity toward 1-phenylethanol increased only marginally from 46.3% at 0.1 MPa to 47.1% at 0.5 MPa. Moreover, at higher hydrogen pressures, overhydrogenation became more evident, increasing the formation of 1-cyclohexylethanol and reducing the chemoselectivity toward 1-phenylethanol to 41.8% at 5.0 MPa.

In contrast, the Pt–HDTMS(30) catalyst achieved complete conversion even at 0.1 MPa and maintained full conversion across the studied pressure range. Notably, Pt–HDTMS(30) preserved a high chemoselectivity of approximately 87.8% toward 1-phenylethanol across all pressure conditions, demonstrating strong resistance to pressure-induced overhydrogenation. This finding suggests that the grafted HDTMS species remained stable even under high hydrogen pressures. Overall, although increasing the hydrogen pressure or increased

Pt loading can improve conversion, both strategies tend to induce overhydrogenation, leading to diminished chemoselectivity toward 1-phenylethanol. In contrast, HDTMS grafting uniquely enables simultaneous enhancement of conversion and chemoselectivity. The observed pressure-dependent trends indicate that HDTMS grafting stabilizes the chemoselective C═O hydrogenation pathway and effectively suppresses pressure-induced overhydrogenation, highlighting its advantage over conventional approaches for improving hydrogenation performance.

Because HDTMS grafting alters the number of exposed Pt sites, conversion alone cannot reflect the intrinsic activity of the Pt–HDTMS(x) catalysts. Therefore, TOFs were analyzed to evaluate the intrinsic activity normalized by the number of CO-accessible Pt atoms (Table 3). The TOF values were calculated from the initial conversion measured within the first 5 min of the reaction (<12%). The ungrafted catalyst exhibited a TOF of 50 h^{-1}, whereas the HDTMS-grafted catalysts showed progressively higher TOF values with increasing grafting amount. Increasing the HDTMS loading from 0.3 to 30 μmol increased the TOF from 267 to 9601 h^{-1}, reflecting a substantial enhancement in intrinsic activity. In particular, Pt–HDTMS(30) achieved a TOF nearly two orders of magnitude higher than that of Pt–HDTMS(0), highlighting the strong promotional effect of HDTMS grafting. Moreover, even when the TOFs were recalculated using the total number of Pt surface atoms, which was identical for all Pt–HDTMS(x) catalysts owing to their similar average NP size of 1.3 nm, the HDTMS-grafted samples exhibited markedly higher intrinsic activity than Pt–HDTMS(0), with Pt–HDTMS(30) showing a TOF approximately 15 times greater (Table S1). These results confirm that the activity enhancement originates from modified catalytic behavior rather than from differences in the number of CO-accessible Pt sites used for normalization.

To further evaluate whether this intrinsic activity enhancement extends beyond acetophenone, a preliminary hydrogenation test was conducted using cinnamaldehyde, an α,β-unsaturated aldehyde containing both C═C and C═O functionalities (Table S2). Consistent with the trends observed for acetophenone, increasing HDTMS grafting markedly enhanced the intrinsic activity for cinnamaldehyde hydrogenation, with the TOF increasing from 26 h^{-1} over Pt–HDTMS(0) to 7039 h^{-1} over Pt–HDTMS(30). Similar trends were obtained when TOFs were normalized using the total number of surface Pt atoms
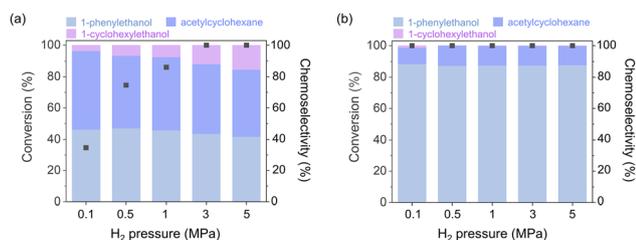

Fig. 5 Conversion and chemoselectivity as functions of hydrogen pressure during acetophenone hydrogenation (measured at 3 h) over (a) Pt–HDTMS(0) and (b) Pt–HDTMS(30).

Table 3 TOF values and chemoselectivity of Pt–HDTMS(x) catalysts in acetophenone hydrogenation

Sample	TOF^a (h^{-1})	Chemoselectivity^b (%)
Pt–HDTMS(0)	50	46.3
Pt–HDTMS(0.3)	267	55.2
Pt–HDTMS(3)	5600	82.8
Pt–HDTMS(30)	9601	88.5

^{a} TOF values determined using the number of exposed Pt sites measured by CO chemisorption. ^{b} Chemoselectivity measured at full conversion.
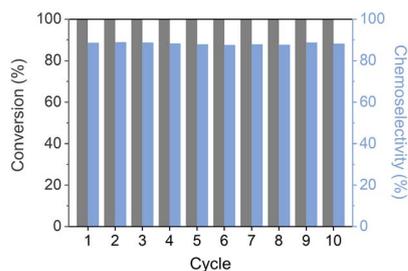
17450 | J. Mater. Chem. A, 2026, 14, 17445–17456

This journal is © The Royal Society of Chemistry 2026

Fig. 6 Reusability test of Pt–HDTMS(30) in acetophenone hydrogenation.

Fig. 7 FTIR transmittance spectra of fresh and spent Pt–HDTMS(30) catalysts over ranges of (a) 3600–2400 cm^{-1} and (b) 1900–1300 cm^{-1}.

Fig. 8 EDS elemental mapping images of spent Pt–HDTMS(30), showing the distributions of (a) Al, (b) O, (c) C, and (d) Pt.

estimated from particle size. In parallel, the C=O chemoselectivity improved from 34.5% to 68.8% with increasing HDTMS loading. Collectively, these results demonstrate that the interfacial HDTMS grafting strategy enhances intrinsic activity while promoting selective carbonyl hydrogenation across structurally distinct multifunctional substrates, supporting the broader applicability of this strategy.

The reusability of Pt–HDTMS(30) was evaluated over 10 consecutive cycles of acetophenone hydrogenation (Fig. 6). After each cycle, the catalyst was recovered by centrifugation, washed with ethanol, and reused under identical reaction conditions. When 30 mg of catalyst was used, the conversion progressively decreased with cycling because of unavoidable catalyst loss during recovery. To minimize this handling-related loss, the reusability test was repeated using 100 mg of catalyst to more reliably assess chemoselectivity retention. Under these conditions, Pt–HDTMS(30) exhibited stable chemoselectivity toward 1-phenylethanol (88.2%) at full conversion over all 10 cycles, confirming its stability. These findings highlight that HDTMS grafting can enable the development of an efficient and durable catalyst suitable for long-term chemoselective hydrogenation.

The structural stability of the spent Pt–HDTMS(30) catalyst after 10 cycles was examined by STEM and XRD. STEM images confirmed that the Pt NPs remained well dispersed with an average size of 1.3 nm, showing no signs of aggregation after repeated use (Fig. S6). This absence of particle aggregation was further supported by XRD, which showed no detectable peaks attributable to crystalline Pt, consistent with the pattern of the fresh Pt–HDTMS(30) catalyst (Fig. S7). Next, the stability of the grafted organic species was examined. FTIR spectra of the spent Pt–HDTMS(30) catalyst showed the same characteristic absorption bands as those of the fresh sample, with C–H stretching and bending vibrations at 2956, 2923, 2851, 1463, and 1385 cm^{-1} (Fig. 7). Although a partial attenuation of the FTIR bands was observed after reuse, the HDTMS-derived functional groups responsible for modulating Pt surface accessibility and catalytic performance were largely retained, consistent with the preserved chemoselectivity of the catalyst. EDS mapping confirmed the retention of the grafted HDTMS species, as evidenced by the persistent carbon signal on the catalyst surface (Fig. 8). ICP and elemental analysis also showed constant Pt loading and only a slight decrease in carbon content after reuse (Table S3). These observations indicate that HDTMS grafting preserves both the structural integrity of Pt NPs and
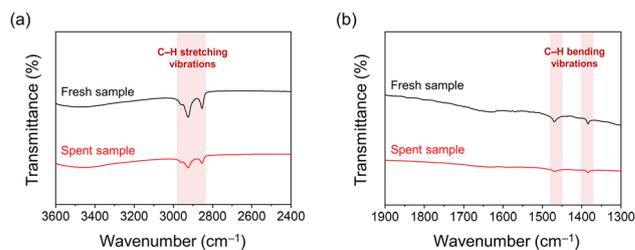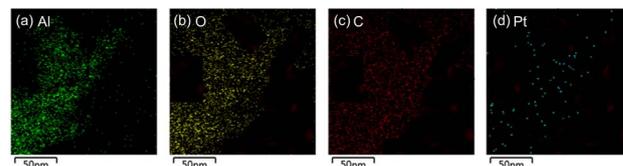
stability of the grafted HDTMS species during repeated operation, thereby enabling sustained catalytic performance over multiple cycles.

Mechanistic origin of the enhanced activity and chemoselectivity of Pt–HDTMS(x)

To elucidate the origin of the enhanced activity and chemoselectivity observed for the Pt–HDTMS(x) catalysts, additional characterizations were performed for the hydrogen activation behavior, Pt surface-site exposure, and possible electronic effects. Given the pronounced differences in conversion between Pt–HDTMS(0) and the HDTMS-grafted catalysts, hydrogen activation was first investigated by H$_2$-TPD (Fig. 9). HDTMS grafting significantly altered the hydrogen activation behavior of the catalysts, providing a mechanistic explanation for the enhanced conversion observed for the Pt–HDTMS(x) series. The ungrafted Pt–HDTMS(0) catalyst displayed a desorption peak ranging from 650 to 900 K, commonly
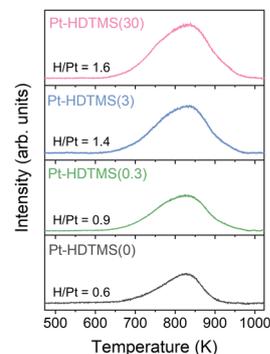

Fig. 9 H$_2$-TPD profiles of Pt–HDTMS(x) catalysts, showing changes in hydrogen desorption behavior with HDTMS loading.

attributable to strongly chemisorbed hydrogen, with a low H/Pt ratio of 0.6. In contrast, the HDTMS-grafted catalysts exhibited broader desorption features spanning 610–980 K, as well as a progressive increase in the H/Pt ratio from 0.9 to 1.6 with increasing HDTMS loading. These results suggest that HDTMS grafting enhances hydrogen activation on the Pt surface.

To further clarify whether the promoted hydrogen availability originates primarily from the modified support surface or from the Pt–organic interfacial environment, additional H_2-TPD control experiments were performed on pristine Al_2O_3, HDTMS(30)–Al_2O_3, and their physical mixtures with Pt–HDTMS(x) catalysts (Fig. S8). Notably, both pristine and HDTMS-treated Al_2O_3 showed no clear H_2 desorption, implying that the support alone does not measurably dissociate or retain hydrogen. In addition, physically mixing HDTMS(30)–Al_2O_3 with Pt–HDTMS(0) or Pt–HDTMS(30) did not generate new desorption components or a meaningful increase in hydrogen uptake; the resulting profiles were comparable to those of the corresponding Pt–HDTMS(x) catalysts. These observations suggest that the modified support does not act as an independent hydrogen reservoir and that the increased hydrogen uptake observed for the HDTMS-grafted catalysts is more plausibly associated with Pt–mediated activation and interfacial effects at the Pt–organic boundary.

Because H_2-TPD primarily reflects changes in hydrogen activation and capacity rather than transport, an additional experiment was conducted to probe hydrogen migration and spillover behavior. A WO_3 color-change experiment was performed under hydrogenation conditions (Fig. S9). Pristine WO_3 exhibited its characteristic bright yellow color. When mixed with Pt–HDTMS(0) and treated under H_2, the powder turned pale green, indicating a slight reduction to partially hydrogenated WO_3 species ($H_\delta WO_3$). In contrast, mixtures containing the HDTMS-grafted catalysts displayed progressively deeper green coloration with increasing HDTMS loading, reflecting the greater extent of WO_3 reduction and providing clear visual evidence of enhanced hydrogen spillover.[39,40] This trend is consistent with the increased hydrogen uptake observed in H_2-TPD and suggests that HDTMS grafting facilitates the mobility of activated hydrogen species beyond the immediate Pt surface.

Taken together, the H_2-TPD and WO_3 experiments indicate that HDTMS grafting modifies both the hydrogen adsorption environment and the mobility of activated hydrogen species. The increased hydrogen uptake and enhanced spillover behavior are consistent with the markedly higher hydrogenation activity of the Pt–HDTMS(x) catalysts, even at low Pt content and under atmospheric H_2 pressure conditions. Similar trends have been reported in previous studies, where increases in hydrogen activation capacity were shown to accelerate hydrogenation kinetics and enhance catalytic turnover.[41–43] These findings support the conclusion that enhanced hydrogen activation and migration collectively contribute to the superior catalytic performance of the HDTMS-grafted catalysts.

These observations are consistent with previous reports of similar phenomena where surface modification or organic grafting has been noted to facilitate hydrogen spillover in metal-oxide systems, thereby enhancing hydrogenation activity by promoting hydrogen delivery to catalytic sites.[44–46] Although the precise atomistic mechanism remains to be further elucidated, the grafted organic species are likely to influence the interfacial environment in a manner that promotes hydrogen transfer between the metal and support. In this context, the organic layer may modify the local diffusion pathway or interfacial energetics, thereby enabling activated hydrogen species to extend beyond the immediate Pt surface. Collectively, the experimental evidence presented here supports an interfacial contribution to the enhanced hydrogen availability and mobility observed in the present system.

In addition to influencing hydrogen activation and migration, HDTMS grafting is expected to alter the distribution of exposed Pt surface sites, which can significantly affect chemoselectivity in structure-sensitive hydrogenation reactions. To examine these surface-site effects, CO-DRIFTS was used to probe how the grafted HDTMS species interact with different Pt coordination environments (Fig. 10). In general, CO adsorption on Pt produces characteristic bands at 2082–2095 cm^{-1} for WC terrace sites and at 2033–2071 cm^{-1} for UC edge and corner sites, enabling the distinction of different Pt surface-site distributions.[47,48] In the present work, the ungrafted Pt–HDTMS(0) catalyst exhibited both WC- and UC-related CO adsorption bands, indicating that all Pt surface sites were accessible. In contrast, the HDTMS-grafted catalysts showed a progressive attenuation of the WC-associated bands at 2082–2095 cm^{-1} with increasing grafting amount, while the UC-related bands remained clearly visible. For Pt–HDTMS(30), the WC features were completely suppressed, indicating selective passivation of terrace sites. A quantitative analysis of the deconvoluted CO-DRIFTS spectra was performed using the previously reported fitting parameters and a relative infrared extinction coefficient of 2.7 for UC sites (Table S4). This analysis revealed a progressive decrease in the WC fraction with increasing HDTMS loading (Table 4). While Pt–HDTMS(0) exhibited WC and UC fractions of 11% and 89%, respectively, the WC component was fully suppressed for Pt–HDTMS(30), confirming exclusive exposure of UC sites. In addition, CO-DRIFTS spectra acquired for Pt–HDTMS(30) after catalysis showed only UC-associated features, with no detectable re-
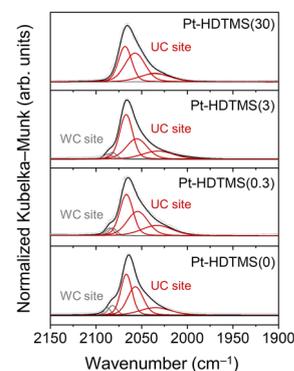

Fig. 10 CO-DRIFTS spectra and corresponding deconvoluted peak profiles for the Pt–HDTMS(x) catalysts.

17452 | J. Mater. Chem. A, 2026, 14, 17445–17456

This journal is © The Royal Society of Chemistry 2026

Table 4 Fractions of WC and UC Pt sites for Pt–HDTMS(x) catalysts, quantified by CO-DRIFTS spectra

Sample	WC sites (%)	UC sites (%)
Pt–HDTMS(0)	11	89
Pt–HDTMS(0.3)	9	91
Pt–HDTMS(3)	8	92
Pt–HDTMS(30)	0	100

emergence of WC features (Fig. S10), indicating that the site modulation was maintained after reaction. Collectively, these results demonstrate that the grafted HDTMS species preferentially interact with and passivate WC Pt sites over UC sites, thereby enabling selective tuning of the Pt NP surface-site environment.

The CO-DRIFTS analysis indicated that HDTMS grafting selectively passivates WC terrace sites and increases the relative exposure of UC sites on Pt surface. In structure-sensitive hydrogenation of aromatic ketones, different Pt surface sites are known to favor distinct adsorption modes.[20,49,50] Aromatic rings generally bind in a flat π-bonded configuration on WC terrace sites, which promotes hydrogenation of the aromatic ring. In contrast, carbonyl groups preferentially adsorb in an end-on configuration on UC sites such as edges and corners, favoring selective C═O hydrogenation. In this context, the progressive masking of WC sites by grafted HDTMS is expected to weaken the adsorption of the aromatic ring of acetophenone and 1-phenylethanol, while preserving efficient activation of the carbonyl group on the remaining UC sites.

As the WC sites become increasingly blocked, the reaction pathway shifts toward selective C═O hydrogenation to form 1-phenylethanol, while the competing aromatic ring hydrogenation (yielding acetylcyclohexane) is strongly suppressed. Further conversion of 1-phenylethanol into 1-cyclohexylethanol, which also requires hydrogenation of the aromatic ring, is likewise inhibited when WC sites are masked by grafted HDTMS. Consequently, both the initial ring-hydrogenation pathway and subsequent overhydrogenation of 1-phenylethanol are effectively prevented. This site-selective modification explains the steady increase in chemoselectivity with increasing HDTMS loading and provides a mechanistic basis for the observation that the Pt–HDTMS(x) catalysts maintain high chemoselectivity even at full conversion and under elevated hydrogen pressures. In particular, WC sites that promote aromatic ring hydrogenation and subsequent overhydrogenation are effectively blocked, whereas the UC sites that drive the desired C═O hydrogenation remain accessible.

To clarify whether the enhanced catalytic behavior observed for the Pt–HDTMS(x) catalysts arises from simple surface coverage or from controlled interfacial effects, a catalyst prepared using the reverse synthetic sequence was examined, in which Pt was first deposited on Al_2O_3 followed by HDTMS grafting, denoted as HDTMS(0.3)–Pt. Catalysts with higher HDTMS loadings in this reverse sequence, such as HDTMS(3)–Pt and HDTMS(30)–Pt, were not considered because HDTMS grafting after Pt deposition resulted in excessive masking of the Pt surface, leading to negligible catalytic activity and preventing meaningful catalytic evaluation. CO chemisorption analysis shows that HDTMS(0.3)–Pt exhibits a substantially lower fraction of surface-accessible Pt sites ($Pt_{avail} = 0.05$) compared with Pt–HDTMS(0.3) ($Pt_{avail} = 0.12$), indicating that HDTMS grafting after Pt deposition leads to more extensive and less controlled masking of the Pt surface (Table S5). Consistent with this observation, the catalytic conversion of HDTMS(0.3)–Pt after 3 h (32.6%) is markedly lower than that of Pt–HDTMS(0.3) (65.6%), reflecting the reduced number of accessible Pt active sites. Despite the reduced activity, the chemoselectivity of HDTMS(0.3)–Pt (54.6%) remains comparable to that of Pt–HDTMS(0.3) (55.2%). CO-DRIFTS spectra show similar WC-related adsorption features for the two catalysts (Fig. S11), consistent with the comparable chemoselectivity observed at low HDTMS loading.

However, the catalytic behavior diverges significantly when higher HDTMS grafting levels are considered. In the grafting-first catalysts, increasing the HDTMS loading progressively enhances chemoselectivity from 55.2% to 82.8% and 88.5% for Pt–HDTMS(3) and Pt–HDTMS(30), respectively, while maintaining high catalytic activity, as reflected by conversions after 3 h of 82.5% and 100%, respectively (Fig. 3 and Table 3). Notably, these catalysts exhibit even larger apparent CO-derived particle sizes ($d_{CO} = 23.6$ and 34.4 nm) than that of HDTMS(0.3)–Pt ($d_{CO} = 19.8$ nm), suggesting more extensive HDTMS-induced surface masking, yet they still maintain significantly higher catalytic activity than the reverse-sequence catalyst. These observations indicate that simple surface coverage alone can partially suppress WC sites and reproduce comparable chemoselectivity at low HDTMS loading. At higher HDTMS loadings, however, the reverse-sequence catalysts suffer from excessive and uncontrolled masking, which substantially limits Pt accessibility and catalytic turnover. In contrast, the grafting-first strategy enables a controlled metal–organic–support interfacial configuration that selectively suppresses WC sites while preserving sufficient Pt accessibility and hydrogen activation capability. Consequently, this interfacial design enables the simultaneous realization of high chemoselectivity and high catalytic activity, highlighting the critical role of controlled interfacial engineering beyond simple surface coverage effects.

To assess whether HDTMS grafting modifies the surface electronic state of Pt NPs, XPS measurements were performed on the Pt–HDTMS(x) catalysts after applying the same H_2 pretreatment used before catalysis (Fig. S12). All samples exhibited Pt^0 species with a Pt $4d_{5/2}$ binding energy centered at 314.5 eV, and no systematic shifts were observed with increasing HDTMS loading.[51,52] These results indicate that HDTMS grafting does not induce a measurable change in the surface electronic state of the Pt NPs, suggesting that the interaction between the HDTMS species and Pt is predominantly geometric rather than electronic in nature. Such behavior is consistent with previous reports showing that, even in the presence of stable organic modification and interfacial

This journal is © The Royal Society of Chemistry 2026

J. Mater. Chem. A, 2026, **14**, 17445–17456 | **17453**

interactions, the electronic structure of metal NPs remains largely unperturbed.[53,54]

The catalytic performance of Pt–HDTMS(x) catalysts can be interpreted in terms of the degree of HDTMS surface coverage and the resulting Pt surface accessibility. As the nominal HDTMS loading increases, the fraction of Pt_{avail} decreases from 0.53 for Pt–HDTMS(0) to 0.12, 0.04, and 0.03 for $x = 0.3$, 3, and 30 μmol, respectively, while the Pt NP size remains unchanged. This indicates that increasing HDTMS coverage progressively restricts Pt surface accessibility without altering intrinsic particle size. At low surface coverage, partial masking of Pt sites leads to moderate improvement in chemoselectivity together with an increase in conversion under identical reaction conditions. At higher surface coverage ($x = 3$–30 μmol), substantial reduction in Pt accessibility is accompanied by pronounced enhancement in chemoselectivity and a marked increase in catalytic activity. The improvement in chemoselectivity is attributed to selective suppression of WC terrace sites, whereas the increased conversion is consistent with enhanced hydrogen uptake and migration, which offset the reduced surface accessibility. In contrast, excessive HDTMS coverage hinders Pt deposition and results in negligible catalytic performance. These observations suggest that optimal catalytic performance arises within a regime of partially restricted Pt surface accessibility, where undesirable WC terrace sites are suppressed while sufficient active sites remain available for catalytic turnover.

These characterizations provide insight into the structural and interfacial origins of the enhanced catalytic performance of the Pt–HDTMS(x) catalysts. H_2-TPD and WO_3-based spillover measurements show that HDTMS grafting increases the availability and mobility of surface hydrogen species. CO-DRIFTS analysis demonstrates that HDTMS selectively blocks WC terrace sites while preserving access to UC sites, thereby modifying the Pt surface-site environment. XPS analysis confirms that these effects result from interfacial and geometric modifications rather than changes in the surface electronic state of Pt. Taken together, these results suggest that enhanced hydrogen activation and selective exposure of UC Pt sites contribute to the improved activity and chemoselectivity of the Pt–HDTMS(x) catalysts.

Although both WC site shielding and enhanced hydrogen migration originate from HDTMS grafting at the metal–support interface, their contributions to catalytic performance can be distinguished based on independent experimental descriptors. The decrease in WC site fraction observed by CO-DRIFTS correlates with the improvement in chemoselectivity toward C=O hydrogenation, indicating that selective WC site suppression governs reaction pathway control. In contrast, the increase in hydrogen uptake quantified by H_2-TPD correlates with the enhancement in intrinsic activity, suggesting that improved hydrogen availability predominantly influences catalytic turnover. Consistent with this interpretation, the reverse-sequence catalyst (HDTMS(0.3)–Pt), in which HDTMS was introduced after Pt deposition, exhibits comparable chemoselectivity but substantially lower catalytic activity due to excessive surface masking, indicating that WC-site suppression alone cannot account for the enhanced activity observed for the grafting-first catalysts. Together, these results demonstrate that surface-site accessibility and hydrogen availability play concurrent yet mechanistically distinguishable roles in determining catalytic chemoselectivity and activity.

Beyond mechanistic clarification, these findings also provide broader implications for catalyst design. While strong metal–support interaction phenomena on reducible oxides regulate metal surface properties through support reduction, the present results show that precise control over surface-site accessibility and hydrogen behavior can be achieved on a non-reducible support through interfacial organic grafting. This interfacial design strategy expands the catalyst design landscape by enabling modulation of surface geometry and hydrogen dynamics without relying on support reducibility.

Conclusion

This study demonstrates that grafting HDTMS onto γ-Al_2O_3 is an effective strategy for enhancing both the activity and chemoselectivity of Pt catalysts toward acetophenone hydrogenation. Despite the low Pt loading of 0.5 wt%, Pt–HDTMS(30) exhibits conversion levels comparable to those of 3Pt–HDTMS(0), which contains sixfold higher Pt loading, while achieving even higher chemoselectivity than 5Pt–HDTMS(0). Based on the combined experimental observations, two key contributions of HDTMS grafting can be identified. First, hydrogen activation and spillover are promoted, leading to increased availability and mobility of activated hydrogen species and supporting high intrinsic activity under mild H_2 conditions. Second, this grafting selectively masks WC terrace sites while retaining access to UC edge and corner sites, thereby altering the distribution of exposed Pt coordination environments in a manner that favors C=O hydrogenation over aromatic-ring hydrogenation, suppressing overhydrogenation. These combined effects allow the Pt–HDTMS(30) catalyst to maintain stable chemoselectivity and activity across a broad range of H_2 pressures and over repeated reaction cycles, with structural integrity confirmed by spectroscopic and microscopic analyses. Overall, interfacial organic grafting can simultaneously modulate hydrogen dynamics and surface-site accessibility, offering a practical design strategy for developing low-metal-loading catalysts with improved efficiency and selectivity. The mechanistic insights presented here provide a foundation for extending organic–inorganic interface engineering concepts to a broader class of structure-sensitive hydrogenation reactions involving multifunctional substrates, and motivate future studies employing *operando* characterization and theoretical modeling to further refine this design strategy.

Author contributions

Minji Yun: conceptualization, investigation, writing – original draft, Hyunjun Jeong: investigation, Dongmin Lee: investigation, Yongju Yun: conceptualization, supervision, writing – review & editing.

17454 | *J. Mater. Chem. A*, 2026, **14**, 17445–17456

This journal is © The Royal Society of Chemistry 2026

Conflicts of interest

There are no conflicts to declare.

Data availability

Supplementary information (SI): N_2 adsorption–desorption isotherms of the Pt–HDTMS(x) catalysts; XRD patterns of Pt, γ-Al_2O_3, Pt–HDTMS(x) and spent Pt–HDTMS(30) catalysts; STEM/EDS images of the Pt–HDTMS(30) and spent Pt–HDTMS(30) catalysts; FTIR transmittance spectrum of HDTMS; product distribution in the hydrogenation of acetophenone over the Pt–HDTMS(x) catalysts; TOF values of the Pt–HDTMS(x) catalysts; catalytic performance of Pt–HDTMS(x) in cinnamaldehyde hydrogenation; Pt and carbon contents of the fresh and spent Pt–HDTMS(30) catalyst; H_2-TPD profiles of supports, Pt–HDTMS(0) and Pt–HDTMS(30) with HDTMS(30)–Al_2O_3; WO_3 color-change experiment photographs of the Pt–HDTMS(x) catalysts; fitting parameters for deconvolution of CO-DRIFTS peaks; CO-DRIFTS for fresh and spent Pt–HDTMS(30) catalysts; Pt properties and catalytic performance of HDTMS(0.3)–Pt catalyst; Pt 4d XPS spectra of the Pt–HDTMS(x) catalysts. See DOI: https://doi.org/10.1039/d5ta10568d.

Acknowledgements

Notes and references

1 Z. Jiang, Y. Zhao, L. Kong, Z. Liu, Y. Zhu and Y. Sun, *ChemPlusChem*, 2014, **79**, 1258–1262.
2 L. Zhang, M. Zhou, A. Wang and T. Zhang, *Chem. Rev.*, 2019, **120**, 683–733.
3 C. Zhu, W. Xu, F. Liu, J. Luo, J. Lu and W. X. Li, *Angew. Chem., Int. Ed.*, 2023, **62**, e202300110.
4 T. Wang, Y. Xin, B. Chen, B. Zhang, S. Luan, M. Dong, Y. Wu, X. Cheng, Y. Liu and H. Liu, *Nat. Commun.*, 2024, **15**, 2166.
5 S. Doherty, J. Knight, T. Backhouse, T. Tran, R. Paterson, F. Stahl, H. Alharbi, T. Chamberlain, R. Bourne and R. Stones, *Catal. Sci. Technol.*, 2022, **12**, 3549–3567.
6 S. Attia and S. Schauermann, *J. Phys. Chem. C*, 2019, **124**, 557–566.
7 F. Meemken and A. Baiker, *Chem. Rev.*, 2017, **117**, 11522–11569.
8 S.-i. Fujita, Y. Onodera, H. Yoshida and M. Arai, *Green Chem.*, 2016, **18**, 4934–4940.
9 Y. Zhang, J. Liu, S. Wang, Z. Yu, H. Zhang, D. Wang, L. Zhu, C. Wu and H. Yu, *Catal. Sci. Technol.*, 2025, **15**, 7244–7250.
10 C.-S. Chen, H.-W. Chen and W.-H. Cheng, *Appl. Catal., A*, 2003, **248**, 117–128.
11 X. Zhang, W. Shi, Y. Li, W. Zhao, S. Han and W. Shen, *ACS Catal.*, 2023, **13**, 4030–4041.
12 H. Liu, G. Lu, Y. Guo, Y. Wang and Y. Guo, *Catal. Commun.*, 2009, **10**, 1324–1329.
13 R. Paul, S. C. Shit, T. Fovanna, D. Ferri, B. S. Rao, G. K. K. Gunasooriya, D. Q. Dao, Q. V. Le, I. Shown and M. P. Sherburne, *ACS Appl. Mater. Interfaces*, 2020, **12**, 50550–50565.
14 N. S. Date, S. E. Kondawar, R. C. Chikate and C. V. Rode, *ACS Omega*, 2018, **3**, 9860–9871.
15 M. Zaarour, J. Cazemier and J. Ruiz-Martínez, *Catal. Sci. Technol.*, 2020, **10**, 8140–8172.
16 H. Zhao, C. Liu, Y. Zheng, S. Li, Y. Gao, Q. Ma, F. Wang and Z. Dong, *ACS Catal.*, 2024, **14**, 8619–8630.
17 K. An and G. A. Somorjai, *ChemCatChem*, 2012, **4**, 1512–1524.
18 X. Du, Y. Huang, X. Pan, B. Han, Y. Su, Q. Jiang, M. Li, H. Tang, G. Li and B. Qiao, *Nat. Commun.*, 2020, **11**, 5811.
19 Y. Kang, J. B. Pyo, X. Ye, T. R. Gordon and C. B. Murray, *ACS Nano*, 2012, **6**, 5642–5647.
20 B. Song, I. Chung, J. Kim, M. Yun and Y. Yun, *J. Catal.*, 2022, **413**, 614–622.
21 Y. Liu, X. Wang, C. Zhang, Q. Xu, L. Dang, X. Zhao, H. Tan, Y. Li and F. Zhao, *New J. Chem.*, 2022, **46**, 15950–15958.
22 M. Li, W. Yin, J. Pan, Y. Zhu, N. Sun, X. Zhang, Y. Wan, Z. Luo, L. Yi and L. Wang, *Chem. Eng. J.*, 2023, **471**, 144691.
23 M. J. Hülsey, V. Fung, X. Hou, J. Wu and N. Yan, *Angew. Chem., Int. Ed.*, 2022, **61**, e202208237.
24 G. Sun, P. Xue, L. Wang, X. Zhang, G. Sun, Z. Wang, Q. Zhang, P. Zhang, Y. Liu and Y. Pan, *Green Chem.*, 2025, **27**, 11739–11768.
25 K. Shun and K. Mori, *Acc. Chem. Res.*, 2025, **58**, 3060–3070.
26 C. A. Schoenbaum, D. K. Schwartz and J. W. Medlin, *Acc. Chem. Res.*, 2014, **47**, 1438–1445.
27 I. Schrader, J. Warneke, J. Backenköhler and S. Kunz, *J. Am. Chem. Soc.*, 2015, **137**, 905–912.
28 P. Liu, R. Qin, G. Fu and N. Zheng, *J. Am. Chem. Soc.*, 2017, **139**, 2122–2131.
29 K. Liu, R. Qin and N. Zheng, *J. Am. Chem. Soc.*, 2021, **143**, 4483–4499.
30 K. R. Kahsar, D. K. Schwartz and J. W. Medlin, *J. Am. Chem. Soc.*, 2014, **136**, 520–526.
31 Y. Zhao, G. Fu and N. Zheng, *Catal. Today*, 2017, **279**, 36–44.
32 Z. Weng and F. Zaera, *J. Phys. Chem. C*, 2014, **118**, 3672–3679.
33 L. Altmann, S. Kunz and M. Bäumer, *J. Phys. Chem. C*, 2014, **118**, 8925–8932.
34 Y. Li, Y. Zhang, K. Qian and W. Huang, *ACS Catal.*, 2022, **12**, 1268–1287.
35 L. R. Baker, G. Kennedy, M. Van Spronsen, A. Hervier, X. Cai, S. Chen, L. W. Wang and G. A. Somorjai, *J. Am. Chem. Soc.*, 2012, **134**, 14208–14216.
36 D. B. Tilley and R. A. Eggleton, *Clays Clay Miner.*, 1996, **44**, 658–664.
37 A. Adamczyk and E. Długoń, *Spectrochim. Acta, Part A*, 2012, **89**, 11–17.
38 N. K. Mishra, C. Kumar, A. Kumar, M. Kumar, P. Chaudhary and R. Singh, *Mater. Sci.-Pol.*, 2015, **33**, 714–718.

This journal is © The Royal Society of Chemistry 2026

J. Mater. Chem. A, 2026, **14**, 17445–17456 | **17455**

39 Z. Gu, M. Li, C. Chen, X. Zhang, C. Luo, Y. Yin, R. Su, S. Zhang, Y. Shen and Y. Fu, *Nat. Commun.*, 2023, **14**, 5836.

40 J. Xu, R. Zhang, K. Wang, X. Wang, S. Song and H. Zhang, *Chem. Res. Chin. Univ.*, 2025, **41**, 15–20.

41 Q. Yang, V. A. Kondratenko, S. A. Petrov, D. E. Doronkin, E. Saraçi, H. Lund, A. Arinchtein, R. Kraehnert, A. S. Skrypnik and A. A. Matvienko, *Angew. Chem., Int. Ed.*, 2022, **61**, e202116517.

42 F. R. Lucci, M. T. Darby, M. F. Mattera, C. J. Ivimey, A. J. Therrien, A. Michaelides, M. Stamatakis and E. C. H. Sykes, *J. Phys. Chem. Lett.*, 2016, **7**, 480–485.

43 L. Xie, J. Liang, L. Jiang and W. Huang, *Chem. Sci.*, 2025, **16**, 3408–3429.

44 Y. Jin, X. Sun, H. Zhong, Z. Cheng, G. Lan, S. Wei, M. Sun, H. Liu and Y. Li, *Appl. Catal. B-Environ. Energy*, 2025, 125980.

45 T. Zhang, J. Luo, Q. Jiang, S. Liang, S. Zhang, K. Zhao, X. Wang, S. Hu, Y. Qin and Z. Gao, *ChemCatChem*, 2025, **17**, e202401721.

46 Y. Li and R. T. Yang, *J. Am. Chem. Soc.*, 2006, **128**, 8136–8137.

47 M. J. Kale and P. Christopher, *ACS Catal.*, 2016, **6**, 5599–5609.

48 T. Avanesian, S. Dai, M. J. Kale, G. W. Graham, X. Pan and P. Christopher, *J. Am. Chem. Soc.*, 2017, **139**, 4551–4558.

49 C. J. Bondue and M. T. Koper, *J. Am. Chem. Soc.*, 2019, **141**, 12071–12078.

50 Y. Zhao, P. Wu, L. Wang, W. Yang, Z. Wang, C. Stampfl, D. He, Y. Luo, A. Baiker and J. Huang, *ACS Catal.*, 2025, **15**, 13916–13928.

51 J. Shyu and K. Otto, *Appl. Surf. Sci.*, 1988, **32**, 246–252.

52 B. Song, D. Lee, H. Jeong, M. Yun and Y. Yun, *ACS Catal.*, 2024, **14**, 2620–2630.

53 Y. Zhao, C. Wang, Y. Liu, D. R. MacFarlane and G. G. Wallace, *Adv. Energy Mater.*, 2018, **8**, 1801400.

54 E. de la Llave, R. Clarenc, D. J. Schiffrin and F. J. Williams, *J. Phys. Chem. C*, 2014, **118**, 468–475.

17456 | *J. Mater. Chem. A*, 2026, **14**, 17445–17456

This journal is © The Royal Society of Chemistry 2026